A productivity collapse to end Earth's Great Oxidation

Malcolm S. W. Hodgskiss[a,1,2], Peter W. Crockford[b,c,1,2], Yongbo Peng[d], Boswell A. Wing[e], and Tristan J. Horner[f,g]

[a]Department of Geological Sciences, Stanford University, Stanford, CA 94305; [b]Department of Earth and Planetary Sciences, Weizmann Institute of Science, 761000 Rehovot, Israel; [c]Department of Geoscience, Princeton University, Princeton, NJ 08544; [d]School of Earth Sciences and Engineering, Nanjing University, 210023 Nanjing, China; [e]Department of Geological Sciences, University of Colorado Boulder, Boulder, CO 80309; [f]Non-traditional Isotope Research on Various Advanced Novel Applications (NIRVANA) Labs, Woods Hole Oceanographic Institution, Woods Hole, MA 02543; and [g]Department of Marine Chemistry & Geochemistry, Woods Hole Oceanographic Institution, Woods Hole, MA 02543

It has been hypothesized that the overall size of—or efficiency of carbon export from—the biosphere decreased at the end of the Great Oxidation Event (GOE) (ca. 2,400 to 2,050 Ma). However, the timing, tempo, and trigger for this decrease remain poorly constrained. Here we test this hypothesis by studying the isotope geochemistry of sulfate minerals from the Belcher Group, in subarctic Canada. Using insights from sulfur and barium isotope measurements, combined with radiometric ages from bracketing strata, we infer that the sulfate minerals studied here record ambient sulfate in the immediate aftermath of the GOE (ca. 2,018 Ma). These sulfate minerals captured negative triple-oxygen isotope anomalies as low as ∼ −0.8‰. Such negative values occurring shortly after the GOE require a rapid reduction in primary productivity of >80%, although even larger reductions are plausible. Given that these data imply a collapse in primary productivity rather than export efficiency, the trigger for this shift in the Earth system must reflect a change in the availability of nutrients, such as phosphorus. Cumulatively, these data highlight that Earth's GOE is a tale of feast and famine: A geologically unprecedented reduction in the size of the biosphere occurred across the end-GOE transition.

Proterozoic | primary productivity | Great Oxidation Event | triple-oxygen isotopes | nutrient limitation

The rise of oxygen in Earth's atmosphere during the early Paleoproterozoic was one of the most transformative events in all of Earth's history. Evidence for this event can be observed through the disappearance of mass-independently fractionated sulfur isotopes (1) within reduced and oxidized forms of sulfur ca. 2,430 to 2,330 Ma (2) as well as macroscale features in the sedimentary record such as the emergence of red beds or the disappearance of detrital pyrite and uraninite (3). Following the initial rise in atmospheric oxygen is the largest positive shift in the carbonate carbon isotope record [∼2,220 to 2,060 Ma (4, 5)] termed the Lomagundi–Jatuli Excursion (LJE). The interval between the initial rise of O_2 ca. 2,430 to 2,330 Ma and the end of the LJE—marked by carbon isotope values returning to values of ∼0‰—has traditionally defined Earth's Great Oxidation Event (6) and we follow this convention here.

The LJE has widely been interpreted as a transient rise in organic carbon burial and by consequence a rise in atmospheric O_2. Importantly, this rise in O_2 has been suggested to exceed not only Archean, but also background Proterozoic (6, 7) and possibly Phanerozoic levels in a so-called "oxygen overshoot" (8, 9). However, this high-O_2 interpretation can be tempered under different assumptions regarding changes in the isotopic value of carbon inputs to the global dissolved inorganic carbon (DIC) reservoir as well as the fractionation associated with carbon fixation by primary producers (10). Moreover, some researchers question whether these ca. 2,220- to 2,060-Ma carbonates actually record changes to global marine DIC and instead have suggested that such isotopic records may document local and/or diagenetic processes (e.g., ref. 11). This controversy surrounding the LJE has motivated independent tests of whether such an oxygen overshoot, and corresponding transition from a high-pO_2 syn-Great Oxidation Event (GOE) state to a comparatively low-pO_2 post-GOE state, even occurred. Numerous independent proxies, while

differing in degree of severity, broadly characterize this interval as a decline in surface environment oxidant inventories (12–18). However, it is worth noting that many such records may better reflect local depositional environments and not necessarily global conditions. Moreover, almost all of these records reflect the passive response of a geochemical proxy to a change in Earth's oxidant reservoir (i.e., the effect), rather than capturing the atmospheric signal of interest or, perhaps more importantly, the underlying cause. Cumulatively, it is clear that the application of an independent test of such models would prove useful in shedding light on the end-GOE transition.

A critical factor in evaluating the GOE and the end-GOE transition is an understanding of the mechanism driving oxygenation. A rise in atmospheric oxygen during the GOE could have been the result of increased organic carbon production (i.e., increased gross primary production [GPP] and by consequence a larger biosphere). To sustain a larger biosphere during both the buildup to and maintenance of a high-pO_2 state during the GOE, it has been proposed that high weathering rates (perhaps including siderite; ref. 9) and consequent phosphorus release would have resulted from elevated H_2SO_4 generation via pyrite oxidation during the GOE (although this remains debated; ref. 12). This large release of phosphorus would have then sustained the posited oxygen overshoot in a feast-like scenario (6, 8). In marked contrast to the elevated GPP hypothesized for the GOE, evidence has been presented that characterizes the mid-Proterozoic [∼2,000 to 1,100 Ma (14)] as an interval of remarkably low GPP, possibly just 6% of modern levels (14, 19). Although GPP changes across this transition have been assumed (16), quantifying the degree to which the GOE deviated from the mid-Proterozoic GPP state remains largely unexplored, and how quickly such a transition in the biosphere occurred to mark the end of the GOE remains unknown. To better understand the end-GOE transition and test the hypothesis that the end-GOE was brought about by a nutrient famine, we

Significance

The Great Oxidation Event (GOE) ca. 2,400 to 2,050 Ma caused the first significant accumulation of free oxygen in the atmosphere and potentially a dramatic growth of oxidant reservoirs on the Earth's surface in a suggested "oxygen overshoot." However, the termination of this event remains poorly understood. Here, we present geochemical data suggesting a drastic decline in gross primary productivity across the end-GOE transition, delineating a shift from "feast" to "famine" conditions characteristic of the next 1 billion y.

employ a combined isotope approach utilizing triple-oxygen ($\Delta^{17}O$), multiple-sulfur ($\delta^{34}S$, $\Delta^{33}S$, $\Delta^{36}S$), and Ba isotopes ($\delta^{138/134}Ba$) on barites collected from the Belcher Group, Nunavut, Canada. These samples capture the interval of time immediately after the GOE (Orosirian; ref. 20) and allow quantitative constraints to be placed on the productivity (GPP) of the biosphere at this time.

Geological Context. The Belcher Group is a 7- to 10-km thick sedimentary basin in subarctic Canada, largely deposited between $2,018.5 \pm 1.0$ Ma and $1,854.2 \pm 1.6$ Ma (Fig. 1 and ref. 20). The lowermost Belcher Group is composed of ~1 km of dolomicrite deposited in a sabkha environment (Kasegalik Formation). This is followed by several hundred meters of Eskimo Formation basalts. Overlying this are 3 km of generally supratidal to shallow subtidal carbonate sedimentary rocks with minor siliciclastic rocks (Fairweather, McLeary, Tukarak, Mavor, Costello, and Laddie formations). Progradation is recorded in the Rowatt and Mukpollo formations, followed by the deposition of granular iron formation in the Kipalu Formation. The overlying Flaherty Formation is composed of submarine basalt and is up to several kilometers thick. The Belcher Group concludes with the deposition of a flysch (Omarolluk Formation) and molasse [Loaf Formation (20–22)].

Evaporite casts and pseudomorphs of SO_4-bearing minerals have been reported in a number of stratigraphic intervals in the Belcher Group and have been further constrained during our fieldwork (Fig. 1 and refs. 22 and 23). In the Kasegalik Formation, chert-replaced gypsum rosettes and crystals are common in dolomicrites, with halite casts occurring more rarely in maroon, argillaceous dolomicrites. Standard heavy mineral separation techniques on 5- to 10-cm thick beds of sandstone from the Kasegalik Formation yielded a small fraction of microbarites (~200 μm in width). No halite was observed in the McLeary Formation but it did bear small chert-replaced, twinned gypsum crystals along a single stratigraphic horizon <2 m thick. Finally, large (~1–4 cm) barite crystals are present in the Costello Formation (22) and are the primary focus of this study. This formation is composed of some 10 to 20 m of gray to black shale, overlain by several hundred meters of rhythmically bedded, variably red, pink, gray, and cream-colored dolomicrite with shale partings and very thinly interbedded limestone. In a small area on eastern Tukarak Island, milky-white barite crystals up to several centimeters in width occur in massive, cream-colored dolomicrite (Fig. 1). There is no evidence for subaerial exposure or the presence of a strongly evaporitic/restricted environment associated with the Costello Formation barites; to the contrary, slumps and partial Bouma sequences have led to the interpretation that the Costello Formation was deposited in a foreslope environment (21).

Mass-Independent Oxygen-Isotope Variations. The $\Delta^{17}O$ anomaly recorded within sedimentary SO_4 reflects both the amount of tropospheric O_2 incorporated into SO_4 during pyrite oxidation [f_{O2}; ~8% to 15% (24)] and the $\Delta^{17}O$ value of ambient tropospheric O_2, which itself is driven by 3 principle variables: pCO_2, pO_2, and GPP (*SI Appendix*, Fig. S2). Photochemical reactions in
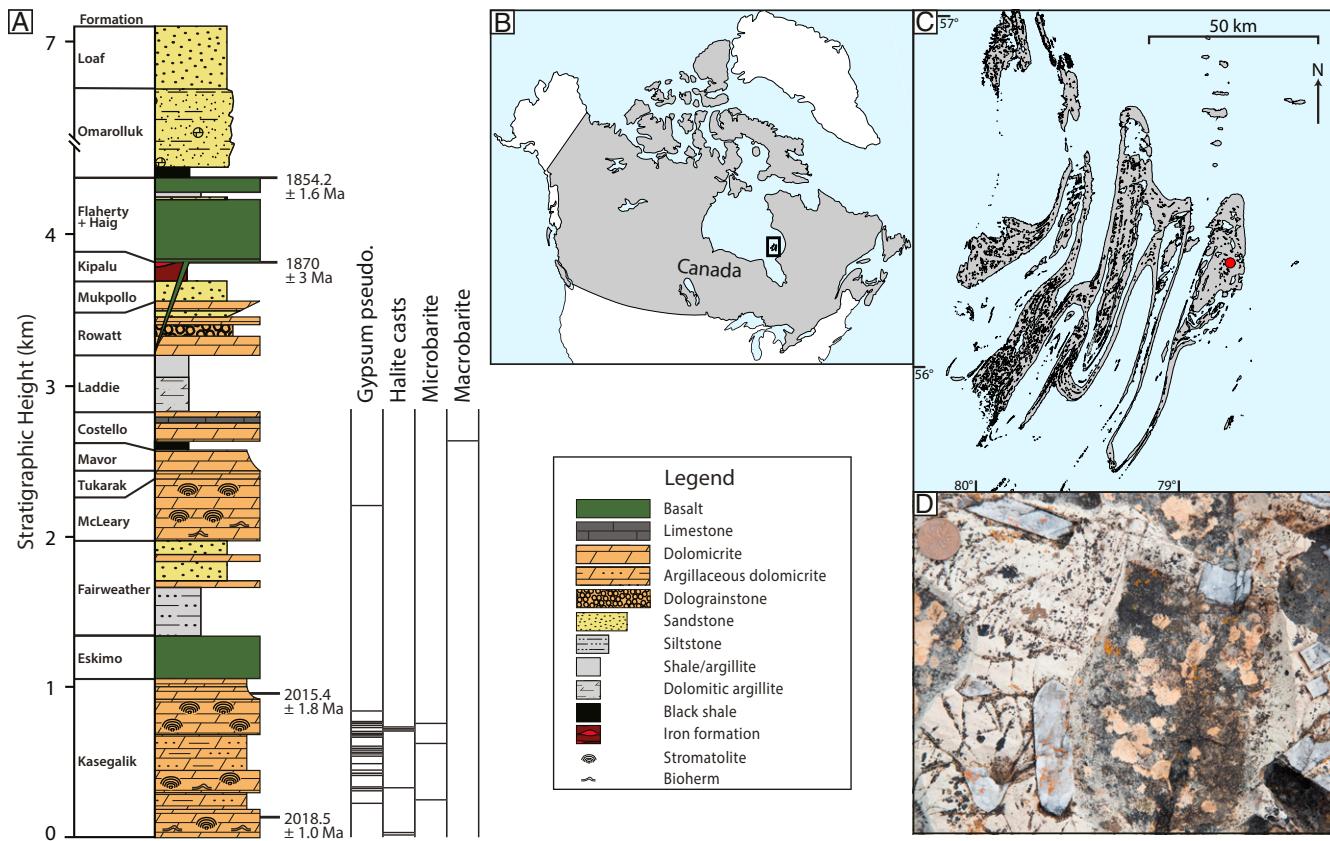
Fig. 1. Location of the Belcher Islands, sampling site, and sulfate/evaporite occurrences. (*A*) Stratigraphic column of the Belcher Group, indicating the intervals at which gypsum pseudomorphs (gypsum pseudo.), halite casts, microbarite, and macrobarite were observed. Refer to *SI Appendix*, Fig. S1 for photographs of each type of occurrence. The Kasegalik Formation, deposited in a sabkha environment, was host to the largest amount of evaporite casts and SO_4 minerals observed in the Belcher Group. Higher in the stratigraphy, the McLeary Formation contains 1 stratigraphic horizon with a small amount of gypsum pseudomorphs. Finally, the Costello Formation contains centimeter-scale barite crystals along a single stratigraphic horizon on eastern Tukarak Island. (*B*) Map of North America with Belcher Islands in the black box. (*C*) Map of Belcher Islands. Macrobarites are indicated by a red circle. (*D*) Macrobarites, with Canadian penny for scale.

the stratosphere involving the production of O_3 (ozone) do so with a mass-independent partitioning of isotopes, where O_3 becomes enriched in ^{17}O and O_2 depleted in ^{17}O, relative to a suggested definition of mass dependence [$\delta^{17}O/\delta^{18}O = 0.5305$ (25, 26)]. Depletions and enrichments in ^{17}O relative to this definition of mass-dependent fractionation are termed "triple-oxygen isotope anomalies," which are defined as $\Delta^{17}O = \delta^{17}O - 0.5305(\delta^{18}O)$ and are reported on the permil (‰) scale relative to Vienna Standard Mean Ocean Water (V-SMOW). The ^{17}O depletion in O_2 (negative $\Delta^{17}O$ values) can be made larger via isotopic exchange between O_3 and CO_2 (27) where larger depletions are observed at higher pCO_2 levels. Mass-independently depleted O_2 produced in the stratosphere is then transported to the troposphere where it is mixed with photosynthetically derived O_2 from the biosphere that carries a mass-dependently fractionated $\Delta^{17}O$ value [i.e., $\Delta^{17}O$ of $\sim$0‰ (ref. 28 and *SI Appendix*, Fig. S2)]. Therefore, the degree of depletion from stratospheric reactions with CO_2, the rate of nonmass independent O_2 production from the biosphere, and the size of the O_2 reservoir where these fluxes compete set the $\Delta^{17}O$ value of tropospheric O_2 (29). Provided that limited amounts of microbial cycling occur, tropospheric $\Delta^{17}O$ values can be deposited and preserved in the sedimentary record in the form of SO_4-bearing minerals (e.g., gypsum, barite, CAS). All postatmospheric processes will shift values toward seawater ($\Delta^{17}O = 0$‰), so $\Delta^{17}O$ values within SO_4-bearing minerals that are more negative than modern tropospheric O_2 ($\Delta^{17}O = -0.516$‰; ref. 30) must have been deposited under different pCO_2-pO_2-GPP conditions than those of the modern environment (14, 19, 29, 31, 32).

Sulfur-Isotope Variations. The sulfur isotopic composition ($\delta^{34}S$, $\Delta^{33}S$) of SO_4-bearing minerals reflects several factors: The isotopic composition of sulfur inputs into the depositional system, which, on long- and short-term timescales is dominated by volcanically and sedimentary-derived sulfur, respectively; the type and intensity of microbial cycling that processes S in SO_4 to HS^- and eventually to pyrite through reactions with Fe in sediments; and any isotopic effects associated with precipitation itself (14, 33). Oxidative weathering of volcanically derived sulfur produces SO_4 with a $\delta^{34}S$ value ($\delta^{34}S = [^{34/32}R_{sample} - {}^{34/32}R_{standard}]/^{34/32}R_{standard}$) of $\sim$0‰ and a $\Delta^{33}S$ value ($\Delta^{33}S = \delta^{33}S - [\delta^{34}S - 1]^{0.515}$) of ~ -0.05‰ (13) reported here relative to Vienna Cañon Diablo Troilite (V-CDT) scale. Fractionation by dissimilatory SO_4 reduction or microbial sulfide oxidation (34), which likely dominated microbial S cycling across the Paleoproterozoic (35), results in sulfide species with lower $\delta^{34}S$ values and thus leaves residual SO_4 isotopically enriched in ^{34}S (e.g., ref. 36). Minor sulfur isotopes are also sensitive to microbial cycling that will slightly increase or decrease $\Delta^{33}S$ values in residual SO_4, depending upon the dominant S metabolism (35–37). Such processes give the modern marine SO_4 reservoir a $\delta^{34}S$ value of $+21.2$‰ and a $\Delta^{33}S$ value of $+0.05$‰ (33). Therefore, multiple sulfur isotopes can aid in exploring the nature of ancient SO_4 deposits (e.g., marine or terrestrial) as well as provide insights into the degree of microbial-S cycling.

Barium-Isotope Variations. Barium stable isotopes, $\delta^{138/134}Ba$, can be used to trace the source and cycling of Ba to modern and ancient barite deposits (e.g., refs. 38 and 39; $\delta^{138/134}Ba = {}^{138/134}Ba_{sample}/^{138/134}Ba_{NIST\ 3104a} - 1$). Broadly speaking, barite formation involves the meeting of 2 segregated fluids at an interface (e.g., ref. 40) or in barite supersaturated microzones within otherwise undersaturated environments (e.g., ref. 41). Barite precipitation favors incorporation of isotopically light Ba with an isotopic effect ~ -0.5‰ (e.g., ref. 41), rendering residual dissolved Ba enriched in "heavy" Ba isotopes by a corresponding amount. Thus, the isotopic composition of Ba in barites is sensitive to the size of the Ba reservoir. Barites produced from semi-infinite "open" reservoirs, such as seawater, exhibit a narrow range of compositions close to the crustal average composition ($\sim$0.0‰ $\pm$ 0.1‰). In contrast, precipitates formed from finite

or "closed" reservoirs, such as cold seeps or hot springs, can exhibit distinctive compositions (38). Such precipitates can exhibit $\delta^{138/134}Ba$ values with a non-0 mean and considerable isotopic variation, which is thought to arise from differences in the isotopic composition of the underlying local Ba source and its respective evolution under semirestricted settings, respectively. Thus, the mean and range of Ba isotope compositions of precipitated barite are broadly indicative of the source of Ba.

Materials and Methods

Nine "macrobarite" samples were collected from the Costello Formation for geochemical analyses. For $\Delta^{17}O$ measurements, samples were dissolved and purified to produce pure barite, which was subsequently lazed and measured by isotope ratio mass spectrometry (IR-MS). For $\delta^{34}S$ and $\Delta^{33}S$ measurements, S was extracted and purified using Thode solution and then fluorinated and measured by IR-MS. Finally, $\delta^{138/134}Ba$ measurements were carried out by sample alkaline dissolution, barium purification using column chromatography, and subsequent analysis by multicollector inductively coupled plasma mass spectrometry. Refer to *SI Appendix* for detailed methods.

Results

Triple-oxygen- and Ba-isotope data for microbarites from the Kasegalik Formation and macrobarites from the Costello Formation along with multiple sulfur isotope data from the Costello Formation are summarized in *SI Appendix*, Table S1. Costello Formation macrobarite $\Delta^{17}O$ values are closely clustered, with all analyses falling between -0.78‰ and -0.55‰, well below that of modern marine SO_4 [-0.09‰ (31)] and modern tropospheric O_2 (-0.516‰; ref. 30 and Fig. 2). $\delta^{34}S$ values in these samples cover a range that includes modern marine SO_4 (33) and overlap with previously published $\delta^{34}S$ CAS values from the Kasegalik Formation (Fig. 3A and ref. 42). Unlike $\delta^{34}S$ values, $\Delta^{33}S$ data significantly deviate from values for modern marine SO_4 [$\Delta^{33}S = +0.05$‰ (33)] with predominantly negative values between -0.11‰ and -0.06‰ (Fig. 3A). Finally, Costello Formation macrobarite $\delta^{138/134}Ba$ data tightly cluster between $+0.08$‰ and $+0.12$‰, similar to values for modern and post-Marinoan marine barites (ref. 38 and Fig. 3B), but contrast with modern terrestrial, cold seep, or hydrothermal values (-0.49‰ to $+0.52$‰, -0.61‰ to $+0.36$‰, and -0.08‰ to -0.04‰, respectively; ref. 38).

Discussion

Genesis of Costello Formation Barites. The Costello Formation is the dominant host of barites (and Ba and SO_4) in the Belcher Group and we explore hypotheses for their genetic origin here. There is no stratigraphic, sedimentologic, mineralogic, or petrographic evidence for subaerial exposure in the Costello Formation (20–22), and thus it is unlikely that the macrobarites formed via direct precipitation of Ba- and SO_4-bearing salts in a strongly evaporitic environment. Rather, their large size, well-developed crystal habit, and lack of preferred orientation with respect to bedding strongly suggest that these barites formed postdepositionally rather than in the water column or at the sediment–water interface with coeval carbonates (Fig. 1). Since barite is an insoluble mineral ($K_{sp} \sim 10$), significant diagenetic accumulations typically require the mixing of 2 separate fluids, one rich in Ba and the other in SO_4 (38, 40). The Ba- and S-isotope composition of barites thus constrains their respective source fluids and enables deduction of the significance of the $\Delta^{17}O$ variations preserved therein.

We consider 5 possible sources of SO_4 to Costello Formation macrobarites. In stratigraphic order these are 1) remobilized SO_4 from the evaporitic and SO_4 pseudomorph-bearing horizons of the Kasegalik Formation, 2) remobilized SO_4 from the microbarite-bearing horizons of the Kasegalik Formation, 3) remobilized SO_4 from the formerly gypsum-bearing horizons of the McLeary Formation, 4) the ambient seawater SO_4 reservoir during the time of Costello Formation deposition, and 5) the downward movement of SO_4 from sediments overlying the Costello Formation. Two of these options (scenarios 2 and 3) can be ruled out on mass-balance grounds. The small stratigraphic expression of the microbarites in
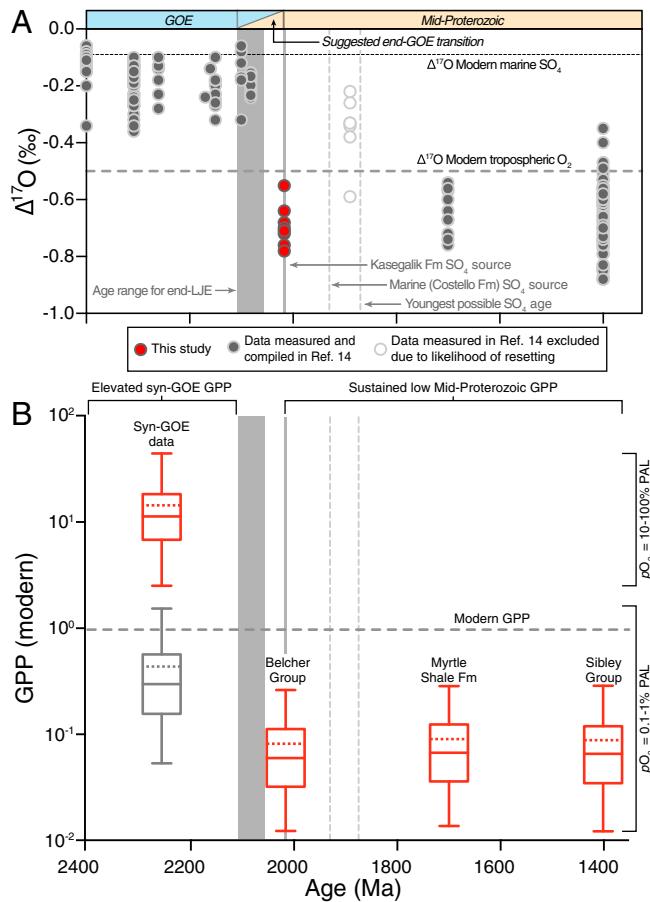
Fig. 2. Geochemical and GPP model results. (*A*) Triple-oxygen isotope results from the Costello Formation macrobarites (red circles) together with results from previously reported values (gray circles) that span the GOE and mid-Proterozoic (ref. 14 and references therein and ref. 46). (*B*) Box and whisker plots for low and high pO_2 scenarios during the GOE and low pO_2 post-GOE, showing the decline in GPP across the end-GOE. GPP fell dramatically across the end-GOE transition, even if pO_2 levels remained constant, and remained at very low levels through the mid-Proterozoic. Bottoms and tops of boxes correspond to 25th and 75th percentiles, respectively. Lower and upper whiskers correspond to 2.5th and 97.5th percentiles, respectively. The solid horizontal lines indicate medians, and dashed horizontal lines indicate means. Dotted vertical lines represent potential SO_4 ages based on different genetic models of barite formation.

the Kasegalik Formation and their low abundance (~1 ppm) make them a poor candidate source of SO_4 to the Costello Formation. Similarly, the McLeary Formation (ca. 1,945 Ma) was observed to have only a very small amount of chert-replaced gypsum. Scenario 5 is also highly unlikely because there are no known occurrences of SO_4-bearing minerals or their pseudomorphs in the stratigraphy overlying the Costello Formation.

The remaining 2 candidate sources of SO_4 set stratigraphically opposed temporal constraints on $\Delta^{17}O$ signatures and, by consequence, Ba. A seawater source of SO_4 (scenario 4) that was penecontemporaneous with deposition of the Costello Formation would imply a more recent origin of the $\Delta^{17}O$ signature, likely imparted ca. 1,930 Ma (assuming a constant sedimentation rate between age constraints), with a minimum age of 1,870 Ma ± 3 Ma from cross-cutting dykes and sills (Fig. 1 and refs. 20 and 43). A diffusive supply of seawater SO_4 to the barite-forming environment would also suggest that the global seawater SO_4 reservoir was characterized by large negative $\Delta^{17}O$ values observed within the macrobarites, given that the Costello Formation bears no evidence for having formed in a strongly hydraulically restricted water mass.

While this scenario is difficult to disprove sedimentologically, it would require abnormally low rates of microbial sulfur cycling to prevent the removal of $\Delta^{17}O$-anomalous SO_4 and abnormally high rates of continental SO_4 inputs to maintain a continuous supply of SO_4 that carried negative $\Delta^{17}O$ anomalies; such a state has been inferred only for the exceptional oceanographic case of a meltwater lens following deglaciation of the Marinoan Snowball Earth (44). The alternative "remobilization" scenario 1, in which the SO_4 in Costello Formation macrobarites was derived from Kasegalik Formation SO_4-bearing minerals, places age constraints between 2,018.5 ± 1.0 Ma and 2,015.4 ± 1.8 Ma on $\Delta^{17}O$ signatures. The Kasegalik Formation contains abundant chert-replaced gypsum pseudomorphs interspersed through some 25% of the stratigraphy (Fig. 1) and therefore, on the grounds of its sheer mass of SO_4-bearing minerals as well as its evaporitic setting, seems a likely source of SO_4 to the overlying Costello Formation. The similarity of $\delta^{34}S$ values of CAS measurements from the Kasegalik Formation (Fig. 3*A* and ref. 42) and those of the macrobarites of the
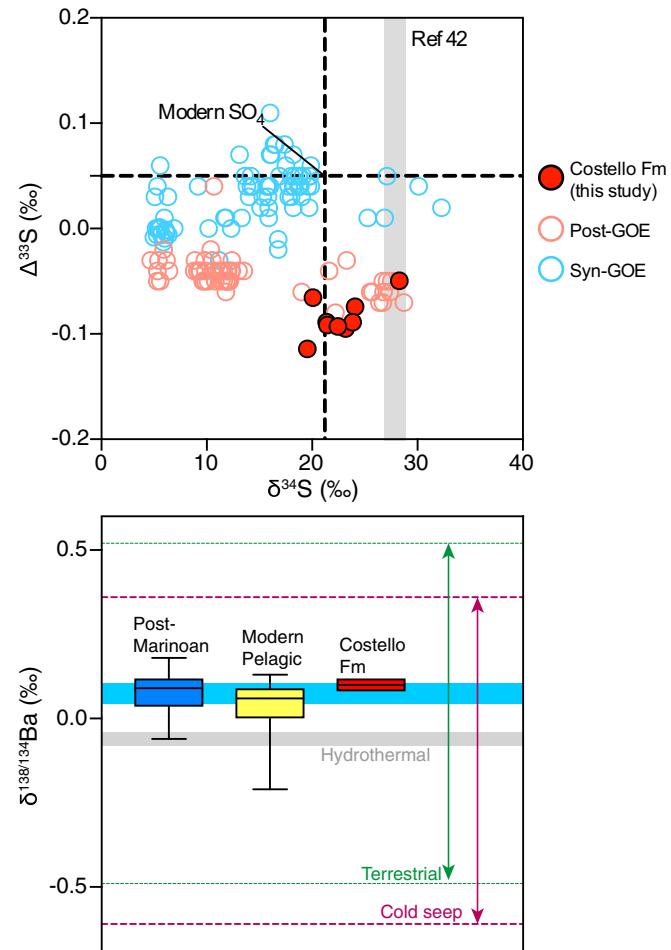

Fig. 3. Sulfur and barium isotope chemistry of Costello Formation macrobarites. (*A*) A $\delta^{34}S$-$\Delta^{33}S$ cross-plot shows that Costello Formation macrobarites are consistently depleted in $\Delta^{33}S$ relative to modern seawater, while they overlap with modern values in $\delta^{34}S$. $\delta^{34}S$ measurements also overlap with CAS measurements of the Kasegalik Formation (gray field; ref. 42). A comparison of syn- to post-GOE sulfate minerals shows that post-GOE samples are comparatively depleted in $\Delta^{33}S$, possibly due to a change in sulfur inputs rather than microbial sulfur recycling. (*B*) $\delta^{138/134}Ba$ measurements of Costello Formation macrobarites compared with potential barite sources and post-Marinoan barites (38). The blue bar represents the typical analytical uncertainty on individual measurements. The range of values and small variance suggest a marine source of Ba for the Costello Formation macrobarites.

Hodgskiss et al.

Costello Formation cannot distinguish between these 2 possibilities, and additional evidence is required to discriminate between these sources of SO_4 for the Costello Formation macrobarites.

As noted previously (e.g., ref. 38), barites precipitated from large Ba reservoirs, such as seawater, generally exhibit a narrow Ba-isotope range close to the crustal average, whereas barites formed in more restricted closed-system settings show wide compositional ranges due to variable influences of inputs, diffusive transport, and precipitation–dissolution events (38). The narrow variance that was measured for $\delta^{138/134}Ba$ values for Costello Formation macrobarites (+0.10‰ ± 0.02‰; ±SD, $n = 7$) is indicative of a large Ba reservoir (e.g., ref. 39). We contend that this reservoir was contemporaneous seawater, since the mean $\delta^{138/134}Ba$ value of Costello Formation macrobarites closely matches those of ancient and modern marine precipitates (41). Due to the insoluble nature of barite, a contemporaneous seawater source of Ba implies a nonseawater source of SO_4 to the Costello Formation macrobarites. In turn, this constraint indicates that Costello Formation macrobarites record $\Delta^{17}O$ anomalies inherited from SO_4 that were tens of millions of years older than the barites themselves (10), which is possible if SO_4-bearing fluids were stored in basinal or crustal brines (40, 45). That is, the remobilized SO_4 originated from the Kasegalik Formation (ca. 2,018.5 ± 0.5 Ma to 2,015.4 ± 1.6 Ma), whereas the Ba source—and thus barite precipitation—possesses a younger age of ca. 1,930 Ma (>1,870 Ma, based on cross-cutting dykes and sills).

A Productivity Crash to End the GOE? $\Delta^{17}O$ values in the Costello Formation macrobarites (with sulfate that formed ca. 2,018.5 to 2,015.4 Ma) are similar to those deposited in the ca. 1,700-Ma Myrtle Shale Formation (14) and ca. 1,400-Ma Sibley Group (19), suggesting that the transition out of the GOE marks the onset of conditions that may have persisted across the >600-My interval separating these deposits (Fig. 2 and refs. 4, 14, 19, and 20). We set temporal constraints on this isotopic transition by comparing Costello Formation macrobarite results to the suggested youngest syn-GOE $\Delta^{17}O$ values from the Tulomozero Formation in Russian Karelia (14, 46). The observation of highly positive $\delta^{13}C$ values (up to +13.9‰) indicates that Tulomozero Formation sulfate was deposited during the LJE, placing an age of at least 2,108 to 2,057 Ma on these sediments and suggesting the shift in $\Delta^{17}O$ values across the end-GOE occurred over <39 to 90 My. This illustrates the relative rapidity of the step change seen in the $\Delta^{17}O$ record across the end-GOE.

The differences in $\Delta^{17}O$ values between syn- and post-GOE samples could indicate a step change in the fraction of atmospheric O_2 preserved within SO_4 deposits (f_{O2}), a step change in the pO_2-pCO_2-GPP conditions that produced the atmospheric $\Delta^{17}O$ anomaly, or some combination of these 2 factors. If the change were only due to f_{O2}, the shift in $\Delta^{17}O$ values across the end-GOE transition would require a >4-fold increase in f_{O2} after the GOE (from >0.02 to <0.15; *SI Appendix*, Fig. S3). However, if pO_2 was lower after the GOE interval (7), one would not expect more O_2 incorporation into SO_4 accompanying sulfide oxidation, thus placing the full burden on enhanced S cycling during the GOE to explain the $\Delta^{17}O$ shift. Both syn- and post-GOE samples exhibit a similar range of $\delta^{34}S$ values (~25‰; Fig. 3A) despite clear interformation variability. This is consistent with a similar degree of S cycling during both intervals and, by inference, no diminution of the syn-GOE $\Delta^{17}O$ signal by enhanced O exchange with water (14, 46). Although the distinctly more positive $\Delta^{33}S$ values in syn-GOE samples could be interpreted to reflect greater S reoxidation at this time (35, 37), another explanation is that the lack of any covariation with $\delta^{34}S$ (cf. refs. 13 and 47) suggests that such signatures might instead reflect an isotopic shift associated with the oxidative weathering of "old" crustal sulfides (48).

In light of these considerations, we explore the $\Delta^{17}O$ transition out of the GOE with respect to changing pO_2-pCO_2-GPP conditions. The spatial and isotopic consistency of the $\Delta^{17}O$ results for the GOE (8 formations; 81 measurements; mean $\Delta^{17}O =$

−0.18‰ ± 0.14‰, 2σ; refs. 14 and 46), as well as for the mid-Proterozoic (3 formations; 86 measurements; mean $\Delta^{17}O =$ −0.68‰ ± 0.25‰, 2σ; refs. 14 and 19), is indicative of a step change in a global process as driving the transition. As a result, we use the Monte Carlo approach of ref. 19, along with independent estimates of pO_2, pCO_2, f_{O2} (24), and other atmospheric parameters (ref. 19 and *SI Appendix*, Table S2), to interpret the $\Delta^{17}O$ record primarily as a monitor of a state shift in GPP. We note that the interpretations presented here are conservative, as S recycling and reoxidation—if they were greater than assumed here—would drive $\Delta^{17}O$ values toward 0 and thus GPP estimates toward higher values.

Across a range of reported pO_2 and pCO_2 conditions for the syn- and post-GOE intervals (*SI Appendix*, Table S3), our calculations show that a dramatic decrease in GPP characterized the end of the GOE. If high pO_2 levels were reached during the GOE (10% to 100% of modern pO_2; ref. 9), which then fell to 0.1% to 1% of modern in the post-GOE interval (7, 49), this transition could reflect a drop in GPP of nearly 200-fold, from a median value of over 1,100% of modern to a median value of ~6% of modern (Fig. 2). This shift reflects the need to dilute a greater standing stock of tropospheric O_2 during the GOE. However, it is unclear whether syn-GOE biogeochemical cycles could support an oxygenic photoautotrophic biosphere that would achieve such high rates of carbon fixation and O_2 production (50, 51). The $\Delta^{17}O$ record may not require such extreme pO_2 levels if their isotopic impact was tempered by some degree of enhanced S recycling and reoxidation during the GOE. A more likely scenario is a moderate transition, from initial pO_2 levels of 1% to 10% of modern to 0.1% to 1% of modern, which would have instead been accompanied by a reduction in GPP of ~10-fold from a median value of ~60% modern to 6% modern (*SI Appendix*, Table S1). Even in the unlikely case that pO_2 levels did not change across the end-GOE, the $\Delta^{17}O$ values reported here still require over a 5-fold decrease in GPP across this transition (Fig. 2). Although our results indicate substantial drops in GPP are necessary to explain the $\Delta^{17}O$ results, there is still a considerable range of possible Earth system states, underscoring the need for additional investigations of how biogeochemical cycles reorganized across the end-GOE transition.

Multiple studies have suggested a larger ocean–atmosphere oxidant inventory over the GOE interval compared with the following 1 billion y of Earth's history (8, 12–18, 52). Interpretations of this decline in oxidant inventory are typified by falling marine SO_4 levels (12–14), as well as a potential decrease in organic carbon burial (50). The $\Delta^{17}O$ evidence presented here suggests that a reduction in GPP may be a common underlying cause of the biogeochemical changes across this interval. This shift in GPP could reflect a change in the availability of critical nutrients, most likely phosphorus (50, 51, 53, 54), to sustain photoautotrophic growth. The switch from a nutrient feast to famine may have resulted from different Fe-P dynamics across this interval (51, 53), perhaps due to the exhaustion of weatherable apatite- and pyrite-rich sediments (8) as well as less P regeneration from biomass that had built up large nutrient reservoirs before the GOE (55). While the most conservative geological constraints limit the duration of this Earth system "tipping point" to <200 My, the geochemical, geochronological, and sedimentological observations reported here point toward a much quicker timescale (<39 to 90 My; Fig. 2) for the end-GOE transition. Cumulatively these findings suggest the end-GOE transition was potentially one of the largest sustained shifts in the productivity of the biosphere, rivaling the colonization of the terrestrial realm by land plants [>2-fold (56)] and the Permo-Triassic mass extinction [>2-fold (32)] and perhaps even approaching the advent of oxygenic photosynthesis [~1,000-fold (57)] in magnitude.

Conclusion. We present data suggesting that the end-GOE transition marks one of the most pronounced sustained changes in the productivity of the biosphere across all of Earth's history. Moreover, our results strengthen the inextricable link between

the ultimate source of oxygen production (the marine biosphere) and the oxidation of the Earth's surface environment. We find a drop in GPP >5-fold, but possibly as much as 2 orders of magnitude across the end-GOE transition using a Monte Carlo approach paired with published estimates of pO_2 and pCO_2. This drop was likely brought about by a large decrease in nutrients supplied to the biosphere that, in turn, marked the conclusion of the GOE and ushered in the subsequent 1-billion-y interval characterized by markedly low and stable GPP compared with the modern Earth. Although the end-GOE is not considered a major biotic event, our results show that the decrease in gross primary productivity across this transition eclipses even the largest extinction events in all of Earth's history.

1. J. Farquhar, H. Bao, M. Thiemens, Atmospheric influence of Earth's earliest sulfur cycle. *Science* **289**, 756–759 (2000).
2. A. P. Gumsley *et al.*, Timing and tempo of the great oxidation event. *Proc. Natl. Acad. Sci. U.S.A.* **114**, 1811–1816 (2017).
3. J. E. Johnson, A. Gerpheide, M. P. Lamb, W. W. Fischer, O_2 constraints from Paleoproterozoic detrital pyrite and uraninite. *Geol. Soc. Am. Bull.* **126**, 813–830 (2014).
4. A. P. Martin, D. J. Condon, A. R. Prave, A. Lepland, A review of temporal constraints for the Palaeoproterozoic large, positive carbonate carbon isotope excursion (the Lomagundi–Jatuli Event). *Earth Sci. Rev.* **127**, 242–261 (2013).
5. M. Schidlowski, R. Eichmann, C. E. Junge, Carbon isotope geochemistry of the Precambrian Lomagundi carbonate province, Rhodesia. *Geochim. Cosmochim. Acta* **40**, 449–455 (1976).
6. H. D. Holland, Volcanic gases, black smokers, and the great oxidation event. *Geochim. Cosmochim. Acta* **66**, 3811–3826 (2002).
7. N. J. Planavsky *et al.*, A case for low atmospheric oxygen levels during Earth's middle history. *Emerging Top. Life Sci.* **2**, 149–159 (2018).
8. A. Bekker, H. D. Holland, Oxygen overshoot and recovery during the early Paleoproterozoic. *Earth Planet. Sci. Lett.* **317**, 295–304 (2012).
9. A. Bachan, L. R. Kump, The rise of oxygen and siderite oxidation during the Lomagundi Event. *Proc. Natl. Acad. Sci. U.S.A.* **112**, 6562–6567 (2015).
10. Y. Miyazaki, N. J. Planavsky, E. W. Bolton, C. T. Reinhard, Making sense of massive carbon isotope excursions with an inverse carbon cycle model. *J. Geophys. Res. Biogeosci.* **123**, 2485–2496 (2018).
11. J. M. Hayes, J. R. Waldbauer, The carbon cycle and associated redox processes through time. *Philos. Trans. R. Soc. Lond. B Biol. Sci.* **361**, 931–950 (2006).
12. N. J. Planavsky, A. Bekker, A. Hofmann, J. D. Owens, T. W. Lyons, Sulfur record of rising and falling marine oxygen and sulfate levels during the Lomagundi event. *Proc. Natl. Acad. Sci. U.S.A.* **109**, 18300–18305 (2012).
13. C. Scott *et al.*, Pyrite multiple-sulfur isotope evidence for rapid expansion and contraction of the early Paleoproterozoic seawater sulfate reservoir. *Earth Planet. Sci. Lett.* **389**, 95–104 (2014).
14. P. W. Crockford *et al.*, Claypool continued: Extending the isotopic record of sedimentary sulfate. *Chem. Geol.* **513**, 200–225 (2019).
15. D. S. Hardisty *et al.*, Perspectives on Proterozoic surface ocean redox from iodine contents in ancient and recent carbonate. *Earth Planet. Sci. Lett.* **463**, 159–170 (2017).
16. D. E. Canfield *et al.*, Oxygen dynamics in the aftermath of the Great Oxidation of Earth's atmosphere. *Proc. Natl. Acad. Sci. U.S.A.* **110**, 16736–16741 (2013).
17. F. O. Ossa *et al.*, Two-step deoxygenation at the end of the Paleoproterozoic Lomagundi Event. *Earth Planet. Sci. Lett.* **486**, 70–83 (2018).
18. M. A. Kipp, E. E. Stüeken, A. Bekker, R. Buick, Selenium isotopes record extensive marine suboxia during the Great Oxidation Event. *Proc. Natl. Acad. Sci. U.S.A.* **114**, 875–880 (2017).
19. P. W. Crockford *et al.*, Triple oxygen isotope evidence for limited mid-Proterozoic primary productivity. *Nature* **559**, 613–616 (2018).
20. M. S. W. Hodgskiss *et al.*, New insights on the Orosirian carbon cycle, early cyanobacteria, and the assembly of Laurentia from the Paleoproterozoic Belcher Group. *Earth Planet. Sci. Lett.* **520**, 141–152.
21. B. D. Ricketts, "Sedimentology and stratigraphy of eastern and central Belcher Islands, Northwest Territories," PhD thesis, Carleton University, Ottawa, ON, Canada (1979).
22. A. G. Sherman, "Anatomy of giant stromatolite mounds in the Paleoproterozoic Mavor Formation, Belcher Islands," N.W.T. M.Sc. thesis, Université de Montreal, Montreal, QC, Canada (1994).
23. R. T. Bell, G. D. Jackson, Aphebian halite and sulphate indications in the Belcher Group, Northwest Territories. *Can. J. Earth Sci.* **11**, 722–728 (1974).
24. N. Balci, W. C. Shanks, B. Mayer, K. W. Mandernack, Oxygen and sulfur isotope systematics of sulfate produced by bacterial and abiotic oxidation of pyrite. *Geochim. Cosmochim. Acta* **71**, 3796–3811 (2007).
25. M. H. Thiemens, J. E. Heidenreich, 3rd, The mass-independent fractionation of oxygen: A novel isotope effect and its possible cosmochemical implications. *Science* **219**, 1073–1075 (1983).
26. J. A. Hayles, X. Cao, H. Bao, The statistical mechanical basis of the triple isotope fractionation relationship. *Geochem. Perspect. Lett.* **3**, 1–11 (2017).
27. J. Wen, M. H. Thiemens, Multi-isotope study of the O (1 D)+ CO_2 exchange and stratospheric consequences. *J. Geophys. Res. Atmos.* **98**, 12801–12808 (1993).
28. B. Luz, E. Barkan, Assessment of oceanic productivity with the triple-isotope composition of dissolved oxygen. *Science* **288**, 2028–2031 (2000).
29. X. Cao, H. Bao, Dynamic model constraints on oxygen-17 depletion in atmospheric O_2 after a snowball Earth. *Proc. Natl. Acad. Sci. U.S.A.* **110**, 14546–14550 (2013).
30. A. Pack *et al.*, Tracing the oxygen isotope composition of the upper Earth's atmosphere using cosmic spherules. *Nat. Commun.* **8**, 15702 (2017).
31. H. Bao, J. R. Lyons, C. Zhou, Triple oxygen isotope evidence for elevated CO_2 levels after a Neoproterozoic glaciation. *Nature* **453**, 504–506 (2008).
32. B. A. Wing, A cold, hard look at ancient oxygen. *Proc. Natl. Acad. Sci. U.S.A.* **110**, 14514–14515 (2013).
33. R. Tostevin *et al.*, Multiple sulfur isotope constraints on the modern sulfur cycle. *Earth Planet. Sci. Lett.* **396**, 14–21 (2014).
34. A. Pellerin *et al.*, Large sulfur isotope fractionation by bacterial sulfide oxidation. *Sci. Adv.* **5**, eaaw1480.
35. M. Kunzmann *et al.*, Bacterial sulfur disproportionation constrains timing of Neoproterozoic oxygenation. *Geology* **45**, 207–210 (2017).
36. B. A. Wing, I. Halevy, Intracellular metabolite levels shape sulfur isotope fractionation during microbial sulfate respiration. *Proc. Natl. Acad. Sci. U.S.A.* **111**, 18116–18125 (2014).
37. D. T. Johnston *et al.*, Multiple sulfur isotope fractionations in biological systems: A case study with sulfate reducers and sulfur disproportionators. *Am. J. Sci.* **305**, 645–660 (2005).
38. P. W. Crockford *et al.*, Barium-isotopic constraints on the origin of post-Marinoan barites. *Earth Planet. Sci. Lett.* **519**, 234–244 (2019).
39. T. J. Horner, C. W. Kinsley, S. G. Nielsen, Barium-isotopic fractionation in seawater mediated by barite cycling and oceanic circulation. *Earth Planet. Sci. Lett.* **430**, 511–522 (2015).
40. J. S. Hanor, Barite–celestine geochemistry and environments of formation. *Rev. Mineral. Geochem.* **40**, 193–275 (2000).
41. T. J. Horner *et al.*, Pelagic barite precipitation at micromolar ambient sulfate. *Nat. Commun.* **8**, 1342 (2017).
42. A. Ueda, E. M. Cameron, H. R. Krouse, 34S-enriched sulphate in the Belcher Group, NWT, Canada: Evidence for dissimilatory sulphate reduction in the early Proterozoic ocean. *Precambrian Res.* **49**, 229–233 (1991).
43. M. Hamilton, K. Buchan, R. Ernst, G. Stott "Widespread and short-lived 1870 Ma mafic magmatism along the northern Superior craton margin" in *Geological Association of Canada Joint Meeting #GA11A-01* (American Geophysical Union, 2009).
44. P. W. Crockford *et al.*, Triple oxygen and multiple sulfur isotope constraints on the evolution of the post-Marinoan sulfur cycle. *Earth Planet. Sci. Lett.* **435**, 74–83 (2016).
45. L. Li *et al.*, Sulfur mass-independent fractionation in subsurface fracture waters indicates a long-standing sulfur cycle in Precambrian rocks. *Nat. Commun.* **7**, 13252 (2016).
46. C. L. Blättler *et al.*, Two-billion-year-old evaporites capture Earth's great oxidation. *Science* **360**, 320–323 (2018).
47. A. Pellerin *et al.*, Mass-dependent sulfur isotope fractionation during reoxidative sulfur cycling: A case study from Mangrove Lake, Bermuda. *Geochim. Cosmochim. Acta* **149**, 152–164 (2015).
48. C. T. Reinhard, N. J. Planavsky, T. W. Lyons, Long-term sedimentary recycling of rare sulphur isotope anomalies. *Nature* **497**, 100–103 (2013).
49. E. J. Bellefroid *et al.*, Constraints on Paleoproterozoic atmospheric oxygen levels. *Proc. Natl. Acad. Sci. U.S.A.* **115**, 8104–8109 (2018).
50. K. Ozaki, C. T. Reinhard, E. Tajika, A sluggish mid-Proterozoic biosphere and its effect on Earth's redox balance. *Geobiology* **17**, 3–11 (2019).
51. T. A. Laakso, D. P. Schrag, Regulation of atmospheric oxygen during the Proterozoic. *Earth Planet. Sci. Lett.* **388**, 81–91 (2014).
52. D. E. Canfield, The early history of atmospheric oxygen: Homage to Robert M. Garrels. *Annu. Rev. Earth Planet. Sci.* **33**, 1–36 (2005).
53. L. A. Derry, Causes and consequences of mid-Proterozoic anoxia. *Geophys. Res. Lett.* **42**, 8538–8546 (2015).
54. T. A. Laakso, D. P. Schrag, Limitations on limitation. *Global Biogeochem. Cycles* **32**, 486–496 (2018).
55. M. A. Kipp, E. E. Stüeken, Biomass recycling and Earth's early phosphorus cycle. *Sci. Adv.* **3**, eaao4795 (2017).
56. C. B. Field, M. J. Behrenfeld, J. T. Randerson, P. Falkowski, Primary production of the biosphere: Integrating terrestrial and oceanic components. *Science* **281**, 237–240 (1998).
57. L. M. Ward, B. Rasmussen, W. W. Fischer, Primary productivity was limited by electron donors prior to the advent of oxygenic photosynthesis. *J. Geophys. Res. Biogeosci.* **124**, 211–226 (2019).